The MUSHA Hand II: A Multi-Functional Hand for Robot-Assisted Laparoscopic Surgery

Huan Liu[1], Mario Selvaggio[1], Pasquale Ferrentino[1], Rocco Moccia[1], Salvatore Pirozzi[2], Umberto Bracale[1], Fanny Ficuciello[1*]

***Abstract*—Although substantial progresses have been made in robot-assisted laparoscopic surgery, the graspers for existing surgical systems generally remain non-sensorized forceps design with limited functions. This paper presents the design, development and preliminary evaluation of the MUSHA Hand II, a multi-functional hand with force sensors for robot-assisted laparoscopic surgery. The proposed hand has three snake-like underactuated fingers that can be folded into a ϕ12 mm cylindrical form. Each finger has a three-axis force sensor, to provide force information. After been deployed into an abdominal cavity, the hand can be configured to either grasper mode, retractor mode or palpation mode for different tasks. Underactuated finger design enhances the adaptivity in grasping and the compliance in interaction with the environment. In addition, fingertip force sensors can be utilized for palpation to obtain a real-time stiffness map of organs. Using the da Vinci Research Kit (dVRK) as a robotic testbed, the functionality of the hand has been demonstrated and experiments have been conducted, including robotic palpation and organ manipulation. The results suggest that the hand can effectively enhance the functionality of a robotic surgical system and overcome the limits on force sensing introduced by the use of robots in laparoscopic surgery.**

***Index Terms*—Robot-assisted laparoscopic surgery, robotic hand, surgical robot, force sensing.**

I. Introduction

ROBOTIC surgical systems can assist surgeons in laparoscopic surgery by offering enhanced visualization of surgical field and better hand-eye coordination. Consequently, hospital stay and mortality of patients can be significantly reduced [1], [2]. Surgical robotics have attracted extensive attention and various robotic systems have been developed. Multi-Port Laparoscopy (MPL) systems include the DLR MiroSurge [3], the Raven-II system [4], the da Vinci Xi system (Intuitive Surgical Inc.), the Senhance Surgical System (TransEnterix Surgical, Inc.) and the Versius system (CMR Surgical Ltd.). Single-Port Laparoscopy (SPL) systems include research prototypes [5]–[8] and commercial ones like the SPORT system (Titan Medical Inc.) and the da Vinci SP system (Intuitive Surgical Inc.). To further minimize invasiveness, Natural Orifice Transluminal Endoscopic Surgery (NOTES) systems have been proposed, such as the systems in [9]–[13] and the commercial Flex system (Medrobotics Co.).

Although some surgical systems demonstrated impressive dexterity, their end-effectors remained similar to the tools for manual laparoscopic surgery. For example, the graspers and fan retractors for the da Vinci surgical system, despite the EndoWrist technology, still use two-jawed forceps-like design. Limited dimension of access port might be the major reason that restricts surgical tools to simple two-jawed design. Another limitation is due to surgical robots' control paradigm that it is still based on teleoperation. As a matter of fact, introducing extra Degrees-of-Freedom (DoF) requires the development of suitable strategies to control them simultaneously [14]–[16].

In certain surgical procedures, large organs need to be retracted for better exposure of the surgical site. For example, in laparoscopic right-sided adrenalectomy or nephrectomy, retraction of the liver is essential for better exposure of the adrenal gland and the kidney [17]. In some cases, to retract the liver from the surgical scene the surgeon uses the jaws of the laparoscopic instrument, exerting high pressure on a small contact area. This task is rather stressful since it has to be repeated several times due to organ/instrument relative slippage. This involves a waste of energy of the surgeon who must repeat this task while performing surgical operations. By the same time, the surgeon limits the contact force on the organ by relying only on visual feedback [18].

Grasping and mobilization of large organs is also necessary for laparoscopic surgeries. For example, bowel mobilization is useful for the identification and dissection of colic or inferior mesenteric vessels during colorectal surgical procedures [19], [20]. Since human organs are generally slippery and existing graspers do not provide prehensile grasp, a high gripping force needs to be applied on the tissue to secure reliable pinch grasp. Inappropriate grasp force may cause tissue injury, especially for handling large organs like the liver, bowel and spleen [21]. Moreover, the missing of tactile sensation of current grasper may worsen the situation, as the surgeon may not know the magnitude of the contact force he/she is applying on the organ via the robotic system.

The introduction of Hand-Assisted Laparoscopic Surgery (HALS) exemplified surgeons' pursuit of dexterity and tactile sensation for laparoscopic surgery [22], [23]. In HALS, surgeon's hand, inserted through an incision on the patient's abdominal wall, offers better manipulation capability and more importantly the tactile sensation. Thus, various operations can be performed, including palpation and gentle manipulation of tissues. Nevertheless, the required $70 - 80$ mm incision may

This project was partially supported by the POR FESR 2014-2020 Italian National program within BARTOLO project CUP B41C17000090007 and by the MIUR PON 2014–2020 Italian National program within PROSCAN project CUP E26C18000170005.

Huan Liu, Mario Selvaggio, Pasquale Ferrentino, Rocco Moccia, Umberto Bracale and Fanny Ficuciello are with the ICAROS Center, University of Naples Federico II, Naples, Italy.

Salvatore Pirozzi is with the University of Campania "Luigi Vanvitelli", Aversa (CE), Italy

$*$ Corresponding author, Email: fanny.ficuciello@unina.it.

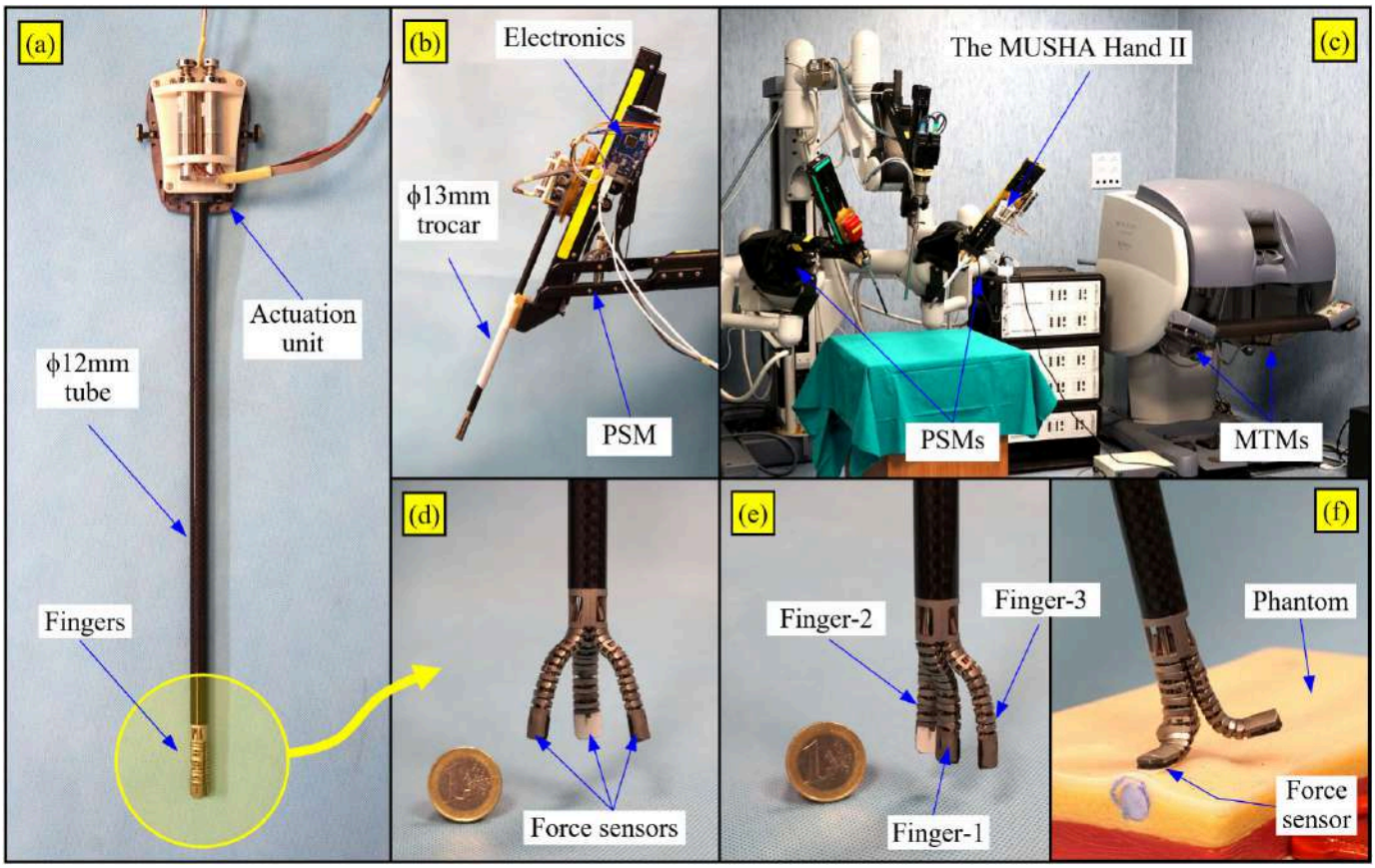

Fig. 1. The developed MUSHA Hand II. (a) The MUSHA Hand II folded to ϕ12 mm cylindrical form. (b) The hand mounted on the PSM of the dVRK system, using the original da Vinci mechanical interface. Electronics is mounted beside. (c) Overview of the hand in the dVRK system. (d) The hand in grasper mode. (e) The hand in fan retractor mode. (f) The hand in palpation mode.

result in increased postoperative pain and wound complications.

The advantages and limitations of HALS lead us to consider that a sensorized multi-functional hand, which can be deployed through a small incision, would offer a surgical system extra dexterity, safe interaction and additional functionalities. However, in comparison to the abundant achievements on robotic surgical systems, the research on multi-functional grasper for robot-assisted surgery have not been paid equivalent attention. This paper attempts to address this shortage.

Few manual multi-phalanx surgical graspers were developed to perform prehensile grasp, including the two-fingered grasper in [21] and three-fingered ones in [24]–[26]. After been deployed into the abdominal cavity, the graspers can be manually operated by surgeons from outside. Although manual graspers might be a cost-effective solution, it brings surgeons extra difficulty to operate and cause extra fatigue.

Motorized hand might be a more ergonomic solution, as the configuration of the hand can be maintained without continuous effort of surgeons. Several motorized tools driven by one to nine motors were proposed [27]–[30]. The required trocar size varies from 10 mm to 45 mm. Although the hands themselves are motorized, a surgeon or extra devices might be needed to hold the device. Furthermore, rigid finger mechanism and lack of tactile feedback might be hidden dangers for laparoscopic surgery.

On the other hand, sensor designs for surgical application have also been investigated, as force sensation offers several advantages for robotic surgery, such as injury reduction [31] and enabling palpation [32]. Force sensors based on different transducer technologies have been proposed, including magnetic [32], optical [33]–[36], resistive [27], [37], [38] and capacitive [39]–[41]. These sensors have been integrated to either conventional two-jawed graspers [36], [38], [39], [41], [42], or specially-designed palpation tools [32], [33], [35], [40] that need to be interchanged during surgery.

Aimed at a miniature multi-functional hand for robot-assisted laparoscopic surgery, the MUSHA (MUltifunctional Smart HAnds) Hand II was developed, as shown in Fig. 1. The MUSHA Hand II is a miniature hand with force sensors for manipulation and palpation of organs in laparoscopic surgery. The hand has three sensorized snake-like fingers, which can be folded together and inserted through a ϕ13 mm trocar. After the insertion, the device can be configured to a grasper, a fan retractor or a palpation tool for different surgical tasks, such as grasping, retraction and palpation. Compared to its previous version [30], the MUSHA Hand II has significant improvements in compactness, integrity and compatibility with the da Vinci Research Kit (dVRK) surgical system.

This paper, presenting the design, development and experimentation of the MUSHA Hand II, is organized as follows. An overview of the hand is briefed in Sect. II. Finger design

and actuation is elaborated in Sect. III, while sensor design and calibration is detailed in Sect. IV. Control hardware and software are presented in Sect. V. Experiments are reported in Sect. VI with the conclusions and future directions summarized in Sect. VII.

II. System Overview

The MUSHA Hand II, designed and developed at the ICAROS center, is shown in Fig. 1. The hand is composed of an actuation unit, three fingers and a ϕ12 mm tube connecting them in between. Its total length is 350 mm, which is close to the length of ordinary da Vinci EndoWrist tools. It is designed for robot-assisted laparoscopic surgery and it can be mounted to one Patient Side Manipulator (PSM) of the dVRK surgical system, as shown in Fig. 1(b) and (c). The hand can be teleoperated by one Master Tool Manipulator (MTM) of the dVRK system.

The hand has three snake-like fingers, which can be folded into a ϕ12 mm cylindrical form, as shown in Fig. 1(a). Thus, the fingers can be inserted through a ϕ13 mm trocar for minimally-invasive surgery. After the insertion, the fingers can be expanded to the grasper mode, the fan retractor mode or the palpation mode for different tasks, as shown in Fig. 1(d), (e) and (f), respectively. The hand has 34 joints in total, including 11 joints for each finger and one joint along the shaft for rotation of all the fingers. The hand is highly-underactuated, as the 34 joints are driven by only six Degrees-of-Actuation (DoA). Underactuated design and integrated elastic elements enable adaptive prehensile grasp. More importantly, the finger is compliant in interaction with organs.

Force sensors are integrated into every fingertips. The sensors provide feedback of the contact force applied on organs to ensure safe interaction. Moreover, once the hand is switched to the palpation mode, the sensors can be employed to palpate tissues, as shown in Fig. 1(f).

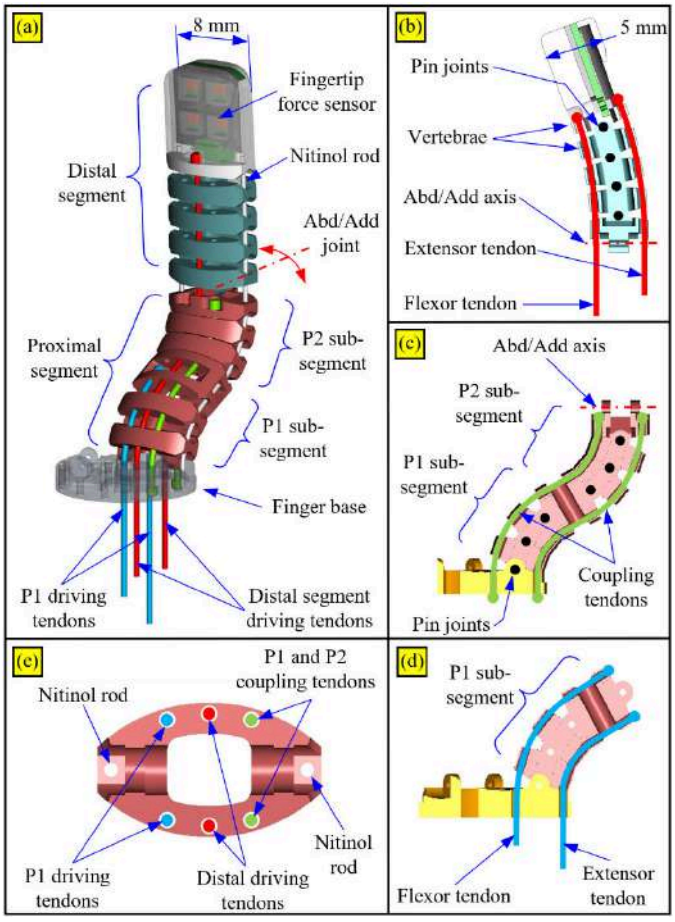

Fig. 2. The underactuated finger design of the MUSHA Hand II. (a) Each finger composed of one proximal segment and one distal segment. The proximal segment can be further divided to two sub-segments. (b) The schematic of the distal segment. (c) The coupling between the P1 and P2 sub-segments. (d) The schematic of the P1 sub-segment. (e) Section view of one vertebra of the P1 sub-segment.

III. Finger Design and Actuation Strategy

A. Underactuated Finger Design

The MUSHA Hand II has three identical fingers evenly spaced at the end of the ϕ12 mm stem, as shown in Fig. 1(d) and (f). Figure 2 shows the design details of one finger. The total length of the finger is 40 mm, while the width and thickness is 8 mm and 5 mm, respectively. Each finger consists of a proximal segment with four joints and a distal segment with five joints. Two segments are connected by a passive abduction/adduction (Abd/Add) joint. Two ϕ0.4 mm nitinol rods are inserted in the holes of each vertebra, from the fingertip to the finger base. Therefore, the Abd/Add joint is compliant, allowing passive rotation of the distal segment between -20° and $+20^\circ$.

The distal segment consists of four vertebrae and one sensorized fingertip, connected by four revolute joints, as shown in Fig. 2(b). The segment is driven by two antagonistic tendons (the red ones) made from ϕ0.4 mm steel cable. The segment can be flexed/extended by pulling the flexor/extensor tendon, respectively. The nitinol rods, arranged at two side of the finger, ensure the tendon actuation is evenly distributed between the four joints when the flexor or the extensor tendon is pulled. In addition, each joint is limited between -20° and $+20^\circ$. Thus, a smooth shape of the segment can be formed. When the hand is commanded to grasp an object, if the proximal vertebra is stopped by the object, the distal joints will continue to flex, leading to a conforming prehensile grasp.

The proximal segment has six vertebrae, which can be further divided into two sub-segments: the P1 sub-segment and the P2 sub-segment. The motions of the P1 and P2 sub-segments are coupled by two tendons (the green ones), as two ends of each tendon are anchored on the hand base and the most distal vertebra of the segment, as shown in Fig. 2(c). Similar to the distal segment of the finger, a pair of antagonistic tendons (the cyan ones) are used to drive the P1 sub-segment, as shown in Fig. 2(d). Therefore, once the P1 sub-segment is bent outward/inward, the P2 sub-segment bends oppositely due to the coupling tendons. Similar design can be found in surgical continuum arm [7]. By this design, the most distal vertebra of the proximal segment remains parallel to the hand base. Hence the distal segment does not need large bending to grasp an object.

All the vertebrae share similar design and Fig. 2(e) presents

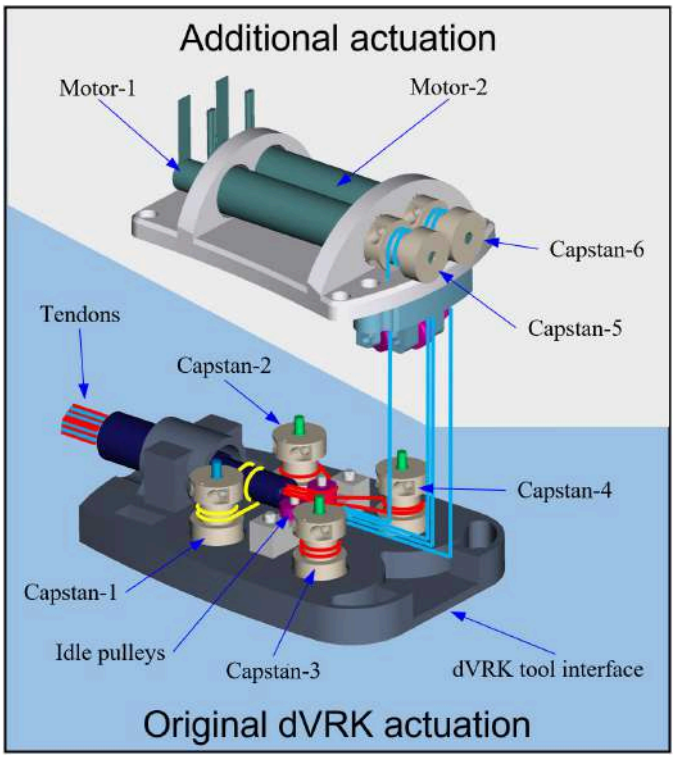

Fig. 3. The actuation unit of the MUSHA Hand II.

a section view of a vertebra of the P1 sub-segment. The vertebrae are hollow inside, allowing the passage of wires for the fingertip sensor. There are eight ϕ0.6 mm holes on each vertebra. The driving tendons of the distal segment (the red dots) go through the two central holes, while the tendons (the cyan dots) for the P1 sub-segment pass the two on the left. The tendons coupling the P1 and P2 sub-segments thread through the holes on the right. On the leftmost and rightmost of the vertebra, there are two holes for the nitinol rods (the white dots).

Using the presented design, each segment is driven by one pair of antagonistic tendons and the actuation of each segment is decoupled. By configuring the three proximal segments the hand can be switched between ϕ12 mm cylindrical form, grasper mode and retractor mode, as shown in Fig. 1(a), (d) and (e) respectively. By driving the distal segments, the hand can perform grasps in the grasper mode. In addition, by extending the distal segments to their limits the hand can be switched to the palpation mode. Thus, the fingertip sensors can be utilized for robotic palpation, as shown in Fig. 1(f).

The snake-like design allows the fingers to always form smooth curves in different configurations. Thus, the hand can be covered by a elastic glove without puncturing it. The use of a disposable glove can make the hand reusable while preventing cross-contamination among patients.

B. Actuation Strategy

The MUSHA Hand II is designed to be tested with the dVRK surgical system. Thus, the actuation unit of the hand was designed based on the original dVRK actuation, as shown in Fig. 3. Considering the compatibility and complexity of the actuation unit, minimal modification has been made to the original dVRK tool interface. Hence, four actuators of the dVRK system could be utilized to drive the hand. In addition, to avoid impairing the gravity-balancing design of the PSM of the dVRK system, minimal number of motors were added to the actuation unit, as shown in Fig. 3. The actuation strategy is summarized in Table 1. The dVRK instrument interface offers four DoA, which drive the four capstans (Capstan-1 to Capstan-4), as shown in Fig. 3. The transmission for the rotation of the shaft remained unchanged, as the Capstan-1 drives the shaft via the yellow tendon. Thus, the whole hand can be rotated along the tool shaft.

TABLE I
ACTUATION STRATEGY OF THE MUSHA HAND II.

Capstan	Driven by	Finger motion
Capstan-1	dVRK	Whole hand rotation along the tool shaft
Capstan-2∼4	dVRK	Distal flexion/extension of the finger-1∼3, respectively
Capstan-5	Motor-1	P1 sub-segment flexion/extension of the Finger-1
Capstan-6	Motor-2	P1 sub-segment flexion/extension of the Finger-2 and -3

The dVRK Capstan-2∼4 drive the flexion/extension of Finger-1∼3 respectively, via the red tendons. As shown in Fig. 3, two motors (Maxon DCX12S 12V with GPX12HP 231:1 gearhead and encoder) were added to drive the proximal segments of the fingers. Capstan-5, mounted on Motor-1, drives the proximal segment of the Finger-1 via one pair of cyan tendons. To simplify the actuation of the hand, the tendons of the proximal segments of Finger-2 and Finger-3 are coupled and driven by Capstan-6 on Motor-2 via one pair of tendons in cyan. By this simplification, the hand can be configured to different configurations (i.e., grasper and retractor modes) using only two motors. The red and cyan tendons are threaded through the ϕ12 mm tube and routed to corresponding fingers via multiple idle pulleys.

The standard tools for robot-assisted laparoscopic surgery usually have four to five DoA, for example four DoA for the Raven II tools and five DoA for the da Vinci XI tools. Therefore, using six DoA is a reasonable choice that will not significantly increase the mechanical and control complexity of a surgical system.

IV. FINGERTIP FORCE SENSOR

A. Design of the Sensors

A developed fingertip force sensor is shown in Fig. 4(a), with a one-EUR coin for dimension reference. The sensor measures 9.5 mm by 8 mm with a thickness of 5 mm, which fits the dimensions of the fingers.

Considering the limited space of the fingertip, a force sensing technology based on optical components and deformable material was adopted [43]. The method uses multiple optical sensible points (called “taxels”) to measure the deformation of

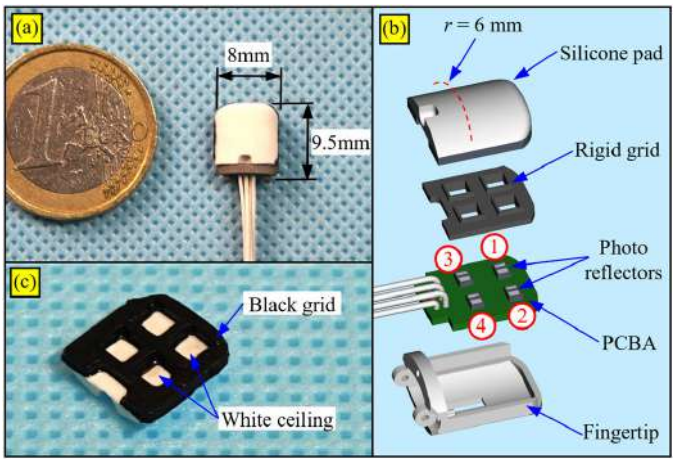

Fig. 4. The three-axis force sensor of the MUSHA Hand II. (a) The sensor dimensions. A one-Euro coin was used for reference of size. (b) The composition of one sensor. (c) The silicone pad.

the elastic layer over the points. After calibration, the signals provided by the taxels can be used to estimate the force applied on the deformable layer.

Figure 4(b) shows the composition of one sensor. A printed circuit board assembly (PCBA) is installed inside a 3D-printed fingertip. On the PCBA, four photo reflectors (NJL5908AR by NJR Corporation, USA) are placed on the PCBA evenly with 3.4 mm distance. Each photo reflector integrates an emitter and a receiver in the same package, which are an infrared Light Emitting Diode (LED) with a peak wavelength at 920 nm and a Photo-Transistor (PT) with a peak wavelength at 880 nm, respectively.

As an object is placed near a photo reflector, the voltage output of the receiver changes according to the distance between the object and the upper surface of the photo reflector. This relationship is non-monotonic according to the datasheet of the reflector. As the distance reduces, the voltage goes up first, then reaches highest voltage at 0.25 mm distance. As the distance further decreases, the voltage drops.

To avoid the non-monotonicity, a 3D-printed rigid grid is introduced between the PCBA and the silicone pad, to prevent the reflection surface reaches 0.25 mm distance. The rigid grid is printed with black plastic to reduce crosstalk.

The silicone pad was cast using silicone molding technology, by using a material with a hardness equal to 20 Shore-A. Moreover, the shape of the pad top side has been designed as a cylinder section with a curvature radius equal to 6 mm (see Fig. 4(b)). Fig. 4(c) shows the bottom side of one pad. The pad has four cells to house the four photo reflectors. The walls are also black to reduce the cross talk between taxels while the ceilings are white to facilitate reflection of infrared light. When an external force is applied on the silicone pad, the pad deforms and the distance between the white surface and the photo reflector changes. Therefore the intensity of the reflected light varies accordingly and the voltage outputs of the photo reflector change.

B. Calibration of the Sensors

To calibrate the sensors, i.e. to obtain the relationship between the applied force and the voltage output of the photo reflectors, sufficient data (about 30,000 pairs of force and voltage data) were collected. Then a neural network was adopted to learn the relationship.

Data were collected using the setup shown in Fig. 5(a). The developed sensor is installed to a reference force sensor (ATI NANO 17 F/T Sensor) by an adapter. The reference sensor is firmly fixed to a workbench. The silicone pad is repeatedly pushed from various directions, using a flat surface of a rigid object. The force measurements of the reference sensor and the voltage signals of the MUSHA Hand II sensor are both recorded using Robot Operating System (ROS), at a sample rate of 180 Hz. For calibration of each fingertip sensor, 180 s of measurements were recorded. Figure 5(b) shows 20 s of the voltage signals from the four taxels of the Finger-1. The voltage outputs of the taxels are about 1 V when no force is applied. When a force is applied, the voltage rise.

The neural network is built and trained using the Neural Networks Toolbox available in MATLAB. The networks for all sensors have the same architecture, chosen experimentally and consisting of one hidden layer with ten neurons and one output layer with three neurons (corresponding to three directions of the contact force). The data of the recorded force and voltage are randomly divided into training, validation, and test subsets comprising 70%, 15%, and 15%, respectively. The weights are randomly initialized using the Nguyen-Widrow rule, and the Levenberg-Marquadt algorithm was used for training.

Figure 5(c), (d) and (e) show the 20 s of force estimated by using the neural network trained for the Finger-1 and the reference ATI sensor. The maximal error on $x-$, $y-$ and $z-$direction is 0.28 N, 0.24 N and 0.75 N, respectively. In this 20 s measurement, the average errors on the three directions are 0.035 N, 0.044 N and 0.116 N, respectively. As indicated by the calibration result, the sensor has higher accuracy and larger range (about 4 N) on the normal direction ($z-$direction).

Note that the estimated force accuracy during the actual use of the sensor in the experiments mainly depends on two aspects: a) the difference among the hardness of actual manipulated object with respect to the one of the object used during the calibration; b) the difference in terms of curvature among these same objects. Both parameters can be suitably designed in order to optimize the sensor for a specific application. In particular, the hardness used for the prototype presented in this paper (20 Shore-A) corresponds to a very soft silicone, and the curvature radius (6 mm) of the pad is quite small. As a consequence, objects that present in the grasping points a local curvature radius sufficiently (almost $4-5$ times) larger with respect to the pad radius can be considered similar to a flat surface with respect to the sensor. Similarly, an object with a hardness sufficiently (almost $4-5$ times) larger with respect to the silicone hardness can be considered similar to a rigid object. Obviously, the closer the local mechanical features of the manipulated object to those used for calibration, the greater the accuracy of the estimated force. For objects far from these conditions a specific calibration should be performed.

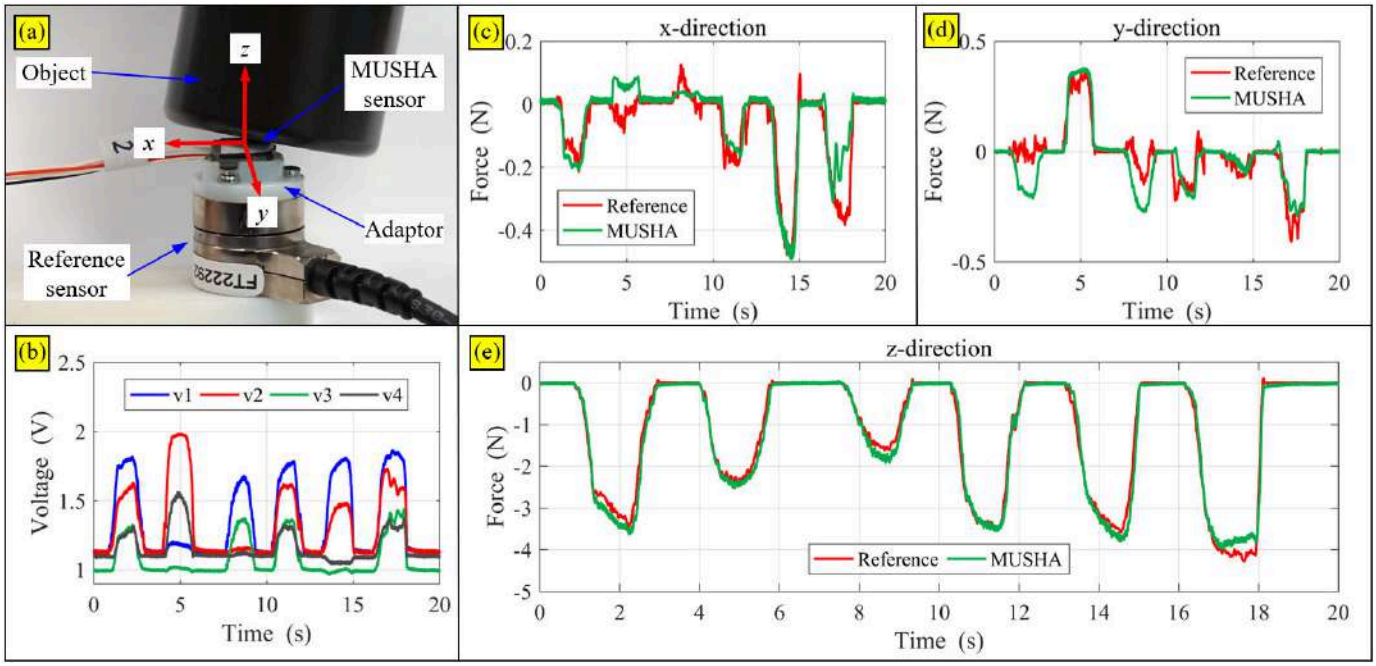

Fig. 5. The calibration of the fingertip force sensor. (a) The setup for data collection. (b) Voltage output of the four taxels during a 20 second test. (c), (d) and (e) The force output of the fingertip sensor, on $x-$, $y-$ and $z-$direction, respectively, compared with the force measurement of the reference sensor.

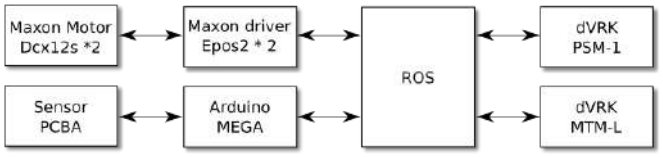

Fig. 6. Software and hardware architecture.

V. Control Hardware and Software

The control architecture (hardware and software) of the hand is schematically depicted in Fig. 6. ROS was used to implement message passing and inter-process communication among different software modules described hereafter.

The Maxon Motor software module communicates with the Maxon drivers (EPOS2 24/2 530239) which provide a read-write interface for the two Maxon motors. The corresponding ROS wrapper provides a set-point command interface for regulating the proximal segments of the hand. The Sensor software module runs on an Arduino Mega and streams a standard wrench ROS topic (containing three force components: one normal and two tangential) for each of the three fingertip sensors. Finally, the dVRK software module consists of a ROS-based layer, which wraps both the MTM and PSM real-time control interfaces, providing sensor measurements (e.g. joint position, velocity and effort) as well as kinematic data through standard ROS topics [44], [45].

The software architecture described so far was used to implement autonomous as well as teleoperation controllers for the MUSHA Hand II control.

For our experimental purposes, we developed a novel teleoperation controller by opportunely modifying the original MTM-PSM teleoperation loop and re-mapping the corresponding Cartesian/joint space commands. More specifically, we mapped the three-dimensional MTM Cartesian displacement $\Delta x_{\text{MTM}} \in \mathbb{R}^3$ to the PSM position commands (by opportunely scaling and rotating the displacement vector from the MTM to the PSM base frame) and implemented a closed-form inverse kinematics function $\text{IK}_{\text{PSM}} : \mathbb{R}^3 \rightarrow \mathbb{R}^3$ to calculate the first three PSM desired actuator values ($\theta_{\text{PSM},1\sim3}$). As for the orientation part, only the seventh joint angle of the MTM ($\theta_{\text{MTM},7}$) was used to command the fourth PSM actuator ($\theta_{\text{PSM},4}$) connected to Capstan-1, which drives the rotation of the whole hand. The three remaining PSM actuators ($\theta_{\text{PSM},5\sim7}$), connected to Capstan-2$\sim$4, drove the distal segments of the MUSHA Hand II fingers through tendons, as explained in Sect. III. These last three motors were jointly and continuously commanded by an opportunely scaled MTM gripper aperture angle ($\theta_{\text{MTM},8}$). For more detailed information about the robot kinematics the interested reader can refer to [46]–[48].

The whole teleoperation architecture is mathematically described by the following set of equations

$$\theta_{\text{PSM}} = \begin{bmatrix} \theta_{\text{PSM},1} \\ \vdots \\ \theta_{\text{PSM},7} \end{bmatrix} = \begin{bmatrix} \text{IK}_{\text{PSM}} \left(p^{\text{off}}_{\text{PSM}} + S_p R^{\text{PSM}}_{\text{MTM}} \Delta x_{\text{MTM}} \right) \\ \Delta\theta_{\text{MTM},7} \\ \theta^{\text{off}}_{\text{PSM}} + S_g \Delta\theta_{\text{MTM},8} \end{bmatrix} \quad (1)$$

where $p^{\text{off}}_{\text{PSM}}, \theta^{\text{off}}_{\text{PSM}} \in \mathbb{R}^3$ are the PSM position and joint offsets, $S_p \in \mathbb{R}^{3\times3}$ and $S_g \in \mathbb{R}^{3\times1}$ are the MTM-PSM coupling scale matrices, and $R^{\text{PSM}}_{\text{MTM}} \in \text{SO}(3)$ denotes the MTM-PSM offset rotation matrix.

To keep the teleoperation control intuitive for the user, we aligned the MTM to the PSM orientation at the beginning of each experiment. The two remaining MTM orientation DoF were thus blocked to the corresponding initial values. The proximal segments of the hand were configured offline by setting the angular values of the two additional Maxton motors

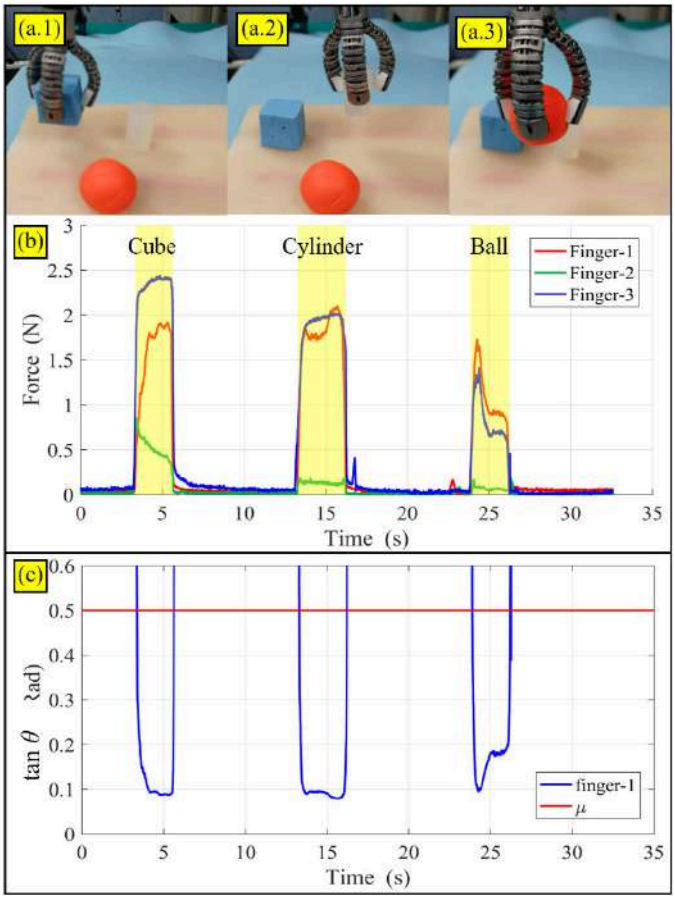

Fig. 7. Rigid object grasping experiment. (a) Snapshots of the hand grasping a cube, a cylinder and a ball. (b) Recorded fingertip force norm for each finger; yellow shaded areas denote time slots in which non-slip grasping condition is met. (c) Trend of $\tan\theta = f_t/f_n$, where θ is the angle between normal and tangential forces; μ is the friction coefficient.

before starting each experiment. In addition, we restored the original dVRK foot pedal-based clutching mechanism that allowed a temporary disconnection between the two sites by re-computing the offsets values. The teleoperation loop ran at 5 ms for testing purposes.

VI. Experiments

This section presents the experiments conducted to verify the idea of introducing a multi-functional hand to robot-assisted laparoscopic surgery.

A. Functionality Demonstration

In this subsection, we demonstrate the functionality of the MUSHA Hand II, including grasping, force sensation, mode switching and interaction compliance. The performance of the hand in clinical context is further presented and evaluated in the following subsections.

In the first set of test, three rigid objects with different material, size and shape were considered, i.e. a rubber cuboid, a plastic cylinder and a plasticine ball as shown in Fig. 7 (a). The grasping forces measured during the proposed grasping experiments are plotted in the graph of Fig. 7 (b). The non-slip condition during grasping writes as $||f_t|| \leq \mu||f_n||$ where f_t, f_n are tangential and normal forces, respectively, and $\mu > 0$ is the friction coefficient. During the teleoperated grasping test, the non-slip condition was verified on each finger and the time slots in which the condition was satisfied are highlighted by the yellow shaded areas. For this experiment, we chose all the objects with masses $m \approx 0.05$ kg and assume a friction coefficient $\mu = 0.5$. As it is possible to note, all the proposed grasps verified the above-mentioned non-slip condition as shown in Fig. 7(c).

The capability of grasping soft and slippery tissues was verified on a swine liver using the teleoperation control described in Sect. V. As shown in Fig. 8(a) and (b), one MTM from the dVRK console was used to teleoperate the MUSHA Hand II mounted on one PSM. The grasp tasks were performed with the vision feedback from the dVRK endoscope. Figure 8(c) shows one frame of the endoscope video.

The hand was first commanded to perform pinch grasps. A small piece of liver was picked up then put down, as shown in the sequence of snapshots in Fig. 8(d). The contact force on Finger-1 was recorded, as shown in Fig. 8(e). Although the maximal contact force is lower than 0.4 N during the operation, the approaching, holding and released phases can still be differentiated from the recorded data. Afterwards, the hand was used to perform prehensile grasps, shown in Fig. 8(f). A relatively bigger and longer piece of liver was successfully grasped using prehensile grasp. At last, the hand was switched to the retractor mode. In this working mode, the hand resembles a fan retractor and it could perform task like pushing organ aside, as shown in Fig. 8(g).

It is worth to note that, due to the underactuated finger design, the fingers of the MUSHA Hand II is compliant during the interaction with soft organs, as shown in Fig. 8(f.3). This feature would be valuable, considering the surroundings of a surgical tool are vulnerable organs.

B. Palpation Experiments

During an open surgery, surgeons can use their hand to locate and diagnose abnormal tissue by direct palpation, as the force feedback from the abnormal and surrounding normal tissue are different. In laparoscopic surgery, direct palpation is not feasible due to the limit incision. In this part of experiment, we attempt to restore the palpation function in robot-assisted laparoscopic surgery using the palpation mode of the sensorized MUSHA Hand II. Compared to using a tool specifically-designed for palpation, using a multi-functional hand may save the time spent on changing the tools.

The hand was configured to the palpation mode shown in Fig. 9(a). The proximal segments were closed, while the distal segments were fully backward bent to the joint limits. The hand was oriented as shown in Fig. 9(a) and the force sensor of the Finger-1 was employed for palpation. In such configuration, the fingertip of Finger-1 is approximately perpendicular to the surface of the phantom. Thus, the measured normal force, which showed larger range in the calibration, can be utilized for precise feedback of the contact force.

A silicone phantom shown in Fig. 9(a) was used for palpation experiment. The side view of the phantom is shown

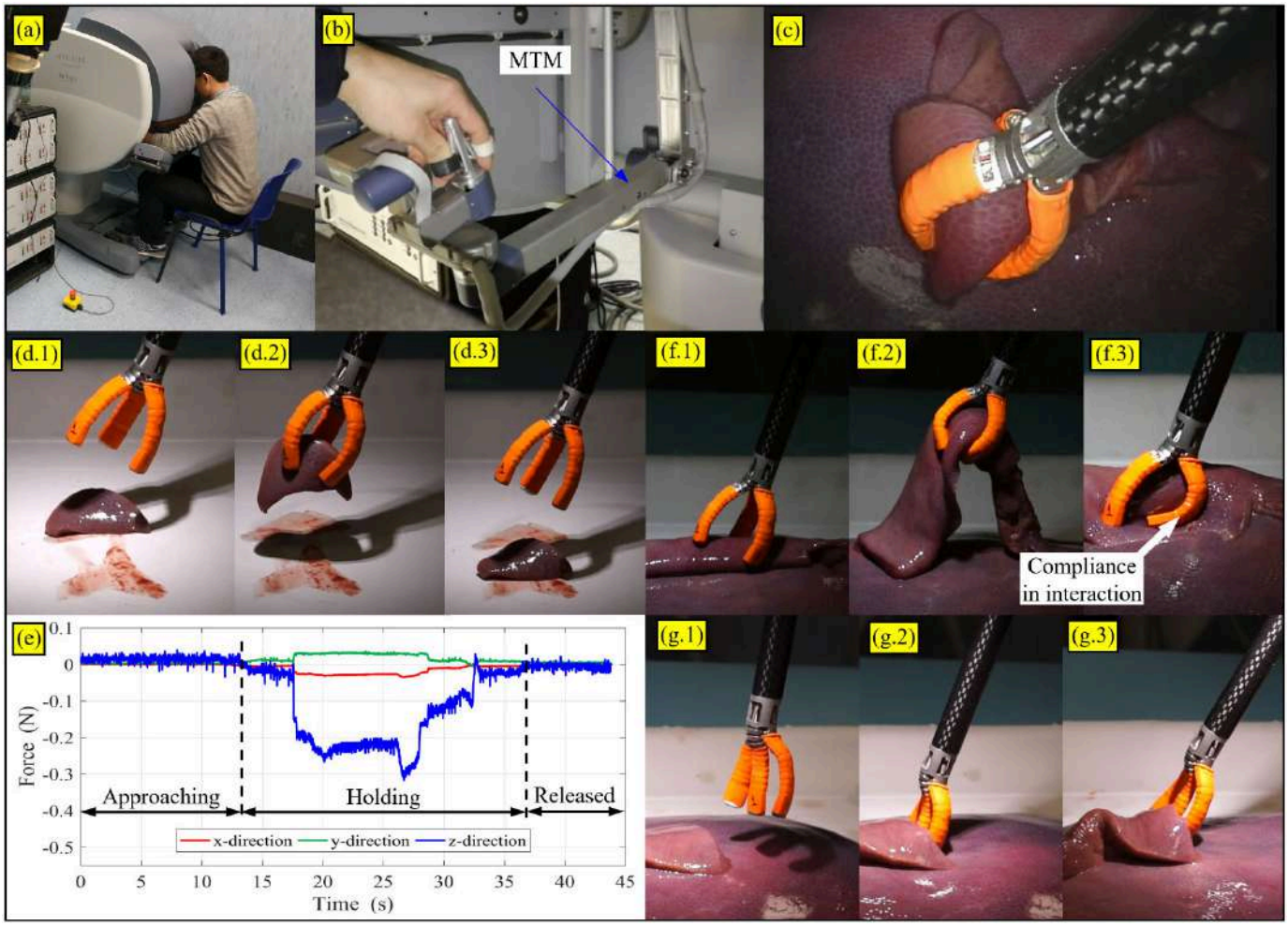

Fig. 8. Functionality demonstration. (a) The hand is teleoperated from the dVRK console. (b) The left MTM is used for controlling the hand. (c) A snapshot of the view from the endoscope. (d) Snapshots of the hand approaching, holding and released a small piece of organ using pinch grasp. (e) Force recorded during the pinch grasp. (f) Snapshots of the hand manipulating bigger piece of organ using prehensile grasp. (g) Snapshots of the hand manipulating the organ using the retractor mode.

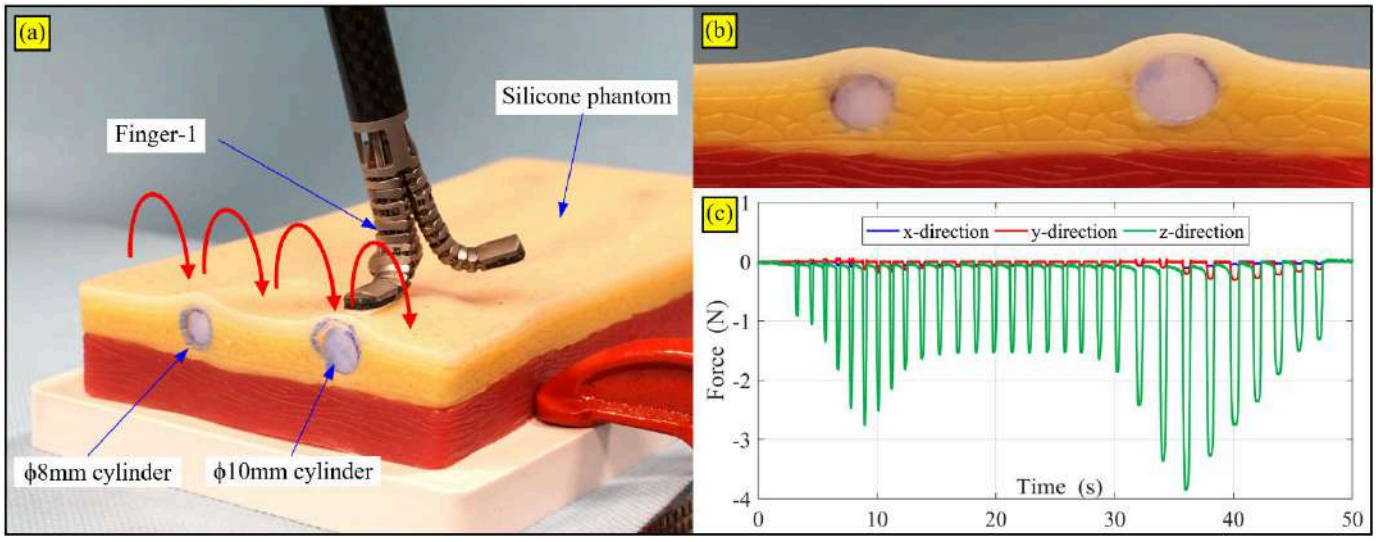

Fig. 9. (a) Setup of the palpation experiment. (b) A side view of the silicone phantom with rigid cylinders inside. (c) The recorded contact force on three directions.

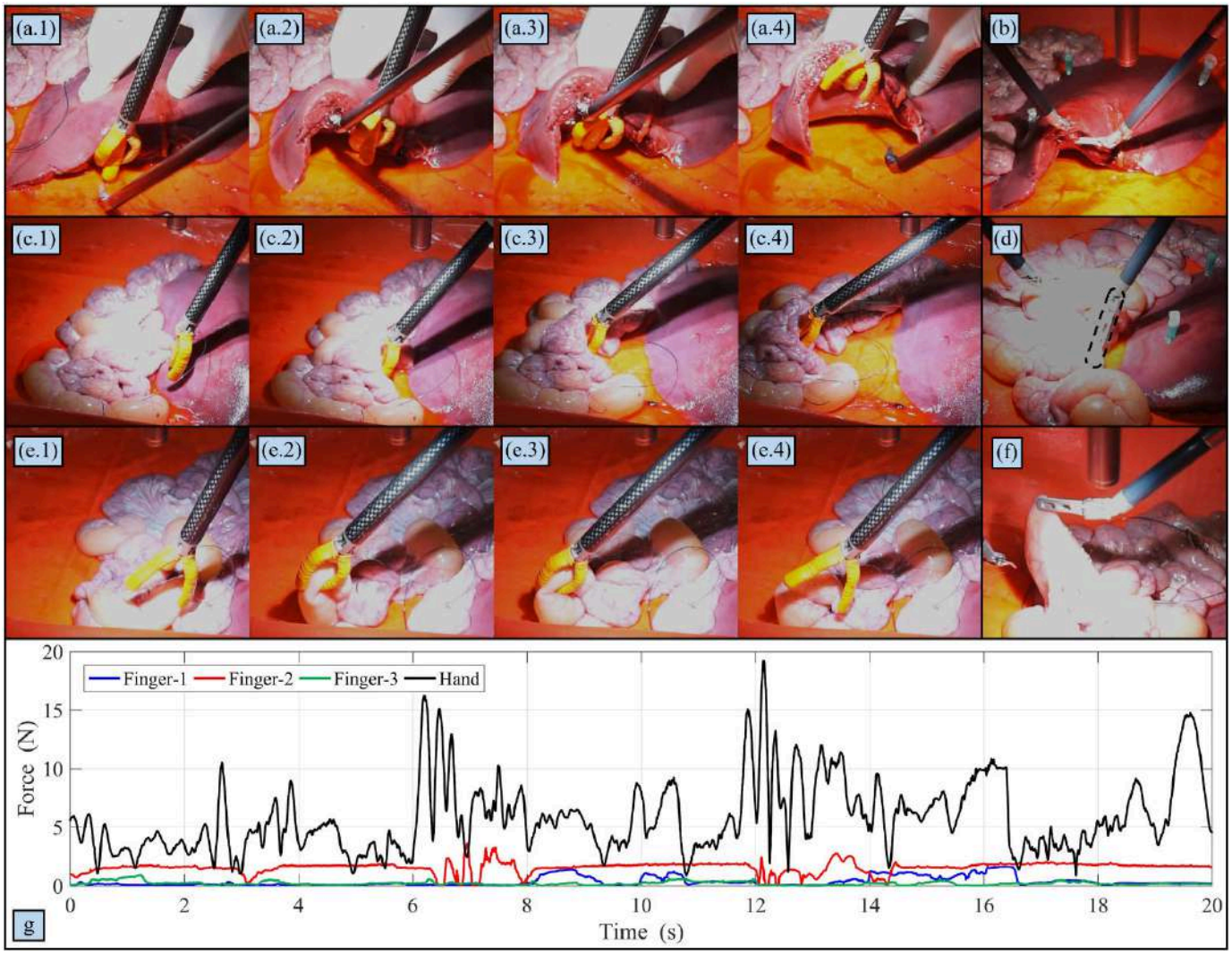

Fig. 10. Manipulation experiments on animal organ. (a) Retraction of the liver using the MUSHA Hand II. (b) Retraction of the liver using the Cadiere forceps. (c) Mobilization of the bowel using the MUSHA Hand II in the retractor mode. (d) Mobilization of the bowel using the Cadiere forceps. (e) Mobilization of the bowel using the MUSHA Hand II in grasper mode. (f) Mobilization of the bowel using the Cadiere forceps. (g) The contact forces measured by the fingertip sensors and the retraction force estimated from the dVRK during the retraction of the liver.

in Fig. 9(b). Two 3D-printed rigid cylinder, with diameters of ϕ8 mm and ϕ10 mm, have been inserted inside the phantom to simulate subserous cancerous tissue.

The hand, autonomously controlled in task space, started from the left of the phantom to palpate point by point. After pressing one point, the hand was lifted and moved to the right for 1.8 mm, towards the next palpation point. Thirty points have been pressed and for each point, the hand lifted and pressed down for the same distance.

The force measurements have been recorded, as shown in Fig. 9(c). When pressing the normal phantom between the two cylinder, the normal force repeatedly reached 1.6 N. When pressing the part with rigid cylinder inside, the force on z-direction reached 2.43 N and 3.91 N for the 8 mm and 10 mm cylinder, respectively. The variation of the tangential force is lower than 0.30 N. Compare to normal part of the phantom, contact force of pressing points with ϕ8 mm and ϕ10 mm rigid inclusion rose 51.9% and 144.4%, respectively. These significant change in contact force could be utilized to identify and locate the abnormal tissue.

C. Manipulation of Animal Organs

The MUSHA Hand II has been further evaluated with a surgeon who is skilled in robot-assisted laparoscopic surgery using commercial da Vinci surgical systems.

As previously mentioned, liver retraction is essential for right-sided adrenalectomy or nephrectomy [17], while bowel mobilization is useful for colorectal procedures [19], [20]. Therefore, the surgeon performed these two typical laparoscopic surgical tasks on a swine liver and bowel, as shown in Fig. 10. Each task has been performed for three times. The experimental setup adopted is the same as the one presented in Fig. 8, with the surgeon controlling the MUSHA Hand II using one MTM. In addition, the same tasks have been performed using commercial EndoWrist Cadiere forceps for comparison.

Figure 10(a) shows the snapshots of the liver retraction using the MUSHA Hand II. Since the liver is laid on a rigid

tray almost seamlessly, the hand could not directly insert under the liver, as shown in Fig. 10(a.1). An EndoWrist needle driver was adopted for assistance, because the needle driver has a sharper tip to wedge under the liver and lift it for about 10 mm, as shown in Fig. 10(a.2). Thereafter, the MUSHA Hand II in the retractor mode further elevated part of the liver from the tray, as presented in Fig. 10(a.3). Finger-2 and 3 were flexed to wedge between the narrow gap lifted by the needle driver. Once the liver was lifted, the fingers were configured to form a fan retractor shape, as shown in Fig. 10(a.4), which offers larger contact surface with a width of approximately 40 mm. On the contrary, as shown in Fig. 10(b), the Cadiere forceps, requiring also the assistance of a needle driver, offered limited contact area that is prone to slippage.

The retractor mode has also been adopted for mobilization of the bowel, as shown in Fig. 10(c). The bowel was consistently pushed to the left in only one move using the MUSHA Hand II (the snapshots of the move are shown in Fig. 10(c.1) to (c.4)). The result suggests that the hand is efficient in achieving an adequate field of view during colorectal procedures. In contrast, using the Cadiere forceps requires multiple moves since they offers smaller contact surface (see Fig. 10(d)) and the bowel covered by mucus is slippery.

Mobilization of the bowel can be also performed using the grasper mode, as shown in Fig. 10(e). The bowel before and after the mobilization is shown in Fig. 10(e.1) and (e.4), respectively, while Fig. 10(e.2) and (e.3) show two snapshots during the mobilization. Due to the snake-like finger design, the hand could perform prehensile grasp on the bowel. Thus, the bowel could be securely lifted and displaced. On the contrary, the Cadiere forceps could perform only pinch grasp. Thus, the bowel was squeezed and the grasp force concentrated on limited contact area, as exemplified in Fig. 10(f).

The interaction force between the organ and each fingertip sensor has been recorded during the test. Fig. 10(g) shows the contact force (combined the components on $x-$, $y-$ and $z-$directions) between the sensors and the liver during the liver retraction. The retraction force of the hand applied on the liver is estimated using the method proposed in [47]. The noise of the force is due to the limited accuracy of the joint position sensors and the friction, elasticity and backlash of the dVRK system, that are difficult to be modeled by the method. As indicated in Fig. 10(g), although the retraction force on the liver reached 19.2 N, the contact forces on the fingertips remained under 3.6 N, suggesting that the retraction force was divided between the fingers, further the fingertips and vertebrae.

The pressure applied on the liver during the retraction can be approximately calculated. The contact area of a fenestrated forcep of the Cadiere measures about 50 mm^2 [49]. If we assume half of the forcep was in contact with the liver, the pressure reached 768 kPa (= 19.2/25 N/mm^2). Similarly, if half of the fingertip of the MUSHA Hand II was in contact with the liver during the retraction, as the area of the fingertip measures about 70 mm^2, the pressure was below 103 kPa (= 3.6/35 N/mm^2). Therefore, the MUSHA Hand II applied much lower pressure on the liver during the retraction, which is about 13.4% of the Cadiere forceps did.

No tissue damage has been detected on the organs after the experiment using either the hand or the forceps. However, the surgeon feels that the MUSHA Hand II is more useful than Cadiere forceps for liver retraction and bowel mobilization, because of its greater contact surface. Particularly, the grasper mode is efficient for grasping and mobilization of the bowel, while the retractor mode is useful for retraction of the liver. In addition, the hand could promptly switch between the two modes by re-configuring the fingers rather than changing the entire instrument.

On the other hand, compared to the Cadiere forceps, the MUSHA Hand II lacks a wrist flexion/extension joint. Thus, the hand does not have the full orientation dexterity, like the Cadiere forceps does. The missing dexterity introduced some difficulty in performing certain tasks. For example, when performing the liver retraction shown in Fig. 10(a), the hand could not be oriented parallel to the tray to facilitate insertion between the liver and the tray. A needle driver was thus adopted for assistance. By adding a wrist flexion/extension joint, the dexterity of the hand can further be enhanced and the needle driver would be spared.

VII. Conclusion and Future Work

Despite the considerable achievements in development of laparoscopic surgical robots, the graspers for the robotic systems have not equally evolved. The widely used devices for organ grasping and manipulation remain non-sensorized forceps design, which has limited performance in manipulation of large organs. In this paper, a multi-functional hand with force sensation was proposed to solve this problem. The developed MUSHA Hand II is a miniature hand for robot-assisted laparoscopic surgery. The hand has multiple snake-like fingers which can provide multi-pattern organ manipulation, such as prehensile grasp and retraction. Fingertip force sensors provide feedback of the contact force, which can be utilized for tissue palpation. Multi-functionality of the MUSHA Hand II has been verified, including palpation of phantom, retraction and mobilization of organs. Benefiting from its multi-functionality, the time spent on changing tools could be saved.

As the potential applications of the hand has been demonstrated, we expect to further optimize the design of the hand for better performance of more surgical tasks and search to transfer the hand to clinical applications. Currently the MUSHA Hand II can rotate along the shaft, which is similar to the the pronation/supination of a human forearm. However, the missing wrist flexion/extension motion, may cause difficulty to place the hand in an orientation for optimal task execution. Further enhancing the dexterity of the miniature hand with respect to surgical constraints, is a valuable direction for further investigation. Moreover, to overcome the limitations related to the presented calibration procedure, in future works two different approaches can be investigated: a) calibrate the sensor with objects having physical properties similar to those to be manipulated during the actual use and train different neural networks corresponding to the different objects; b) design and install three sensors on the same device with different curvatures and hardness. These two approaches can be evaluated also in combination.

REFERENCES

[1] M. J. Mack, "Minimally invasive and robotic surgery," *The Journal of the American Medical Association*, vol. 285, no. 5, pp. 568–572, 2001.

[2] M. Salman, T. Bell, J. Martin, K. Bhuva, R. Grim, and V. Ahuja, "Use, cost, complications, and mortality of robotic versus nonrobotic general surgery procedures based on a nationwide database," *The American Surgeon*, vol. 79, no. 6, pp. 553–560, 2013.

[3] S. Thielmann, U. Seibold, R. Haslinger, G. Passig, T. Bahls, S. Jörg, M. Nickl, A. Nothhelfer, U. Hagn, and G. Hirzinger, "MICA - a new generation of versatile instruments in robotic surgery," in *2010 IEEE/RSJ International Conference on Intelligent Robots and Systems*, 2010.

[4] B. Hannaford, J. Rosen, D. W. Friedman, H. King, P. Roan, L. Cheng, D. Glozman, J. Ma, S. N. Kosari, and L. White, "Raven-II: An open platform for surgical robotics research," *IEEE Transactions on Biomedical Engineering*, vol. 60, no. 4, pp. 954–959, 2013.

[5] G. Petroni, M. Niccolini, A. Menciassi, P. Dario, and A. Cuschieri, "A novel intracorporeal assembling robotic system for single-port laparoscopic surgery," *Surgical Endoscopy*, vol. 27, no. 2, pp. 665–670, 2013.

[6] J. Lee, J. Kim, K.-K. Lee, S. Hyung, Y.-J. Kim, W. Kwon, K. Roh, and J.-Y. Choi, "Modeling and control of robotic surgical platform for single-port access surgery," in *IEEE/RSJ International Conference on Intelligent Robots and Systems*, 2014, pp. 3489–3495.

[7] K. Xu, J. Zhao, and M. Fu, "Development of the sjtu unfoldable robotic system (SURS) for single port laparoscopy," *IEEE/ASME Transactions on Mechatronics*, vol. 20, no. 5, pp. 2133–2145, 2015.

[8] S. Matich, C. Neupert, A. Kirschniak, H. F. Schlaak, and P. P. Pott, "A new single-port robotic system based on a parallel kinematic structure," in *IEEE/RSJ International Conference on Intelligent Robots and Systems*, 2015, pp. 236–241.

[9] S. Phee, S. Low, Z. Sun, K. Ho, W. Huang, and Z. Thant, "Robotic system for no-scar gastrointestinal surgery," *The International Journal of Medical Robotics and Computer Assisted Surgery*, vol. 4, no. 1, pp. 15–22, 2008.

[10] A. C. Lehman, J. Dumpert, N. A. Wood, L. Redden, A. Q. Visty, S. Farritor, B. Varnell, and D. Oleynikov, "Natural orifice cholecystectomy using a miniature robot," *Surgical Endoscopy*, vol. 23, no. 2, pp. 260–266, 2009.

[11] G. Tortora, A. Dimitracopoulos, P. Valdastri, A. Menciassi, and P. Dario, "Design of miniature modular in vivo robots for dedicated tasks in minimally invasive surgery," in *IEEE/ASME International Conference on Advanced Intelligent Mechatronics*, 2011, pp. 327–332.

[12] J. Zhao, X. Zheng, M. Zheng, A. J. Shih, and K. Xu, "An endoscopic continuum testbed for finalizing system characteristics of a surgical robot for notes procedures," in *2013 IEEE/ASME International Conference on Advanced Intelligent Mechatronics*, 2013, pp. 63–70.

[13] R. J. Hendrick, C. R. Mitchell, S. D. Herrell, and R. J. Webster III, "Hand-held transendoscopic robotic manipulators: A transurethral laser prostate surgery case study," *International Journal of Robotics Research*, vol. 34, no. 13, pp. 1559–1572, 2015.

[14] F. Ficuciello, "Synergy-based control of underactuated anthropomorphic hands," *IEEE Transactions on Industrial Informatics*, vol. 15, no. 2, pp. 1144–1152, 2019.

[15] F. Ficuciello, A. Federico, V. Lippiello, and B. Siciliano, "Synergies evaluation of the SCHUNK S5FH for grasping control," in *Advances in Robot Kinematics*, J. Lenarčič, JP. Merlet (Eds.), Springer Proceedings in Advanced Robotics, vol. 4, 2016.

[16] F. Ficuciello, G. Tamburrini, A. Arezzo, L. Villani, and B. Siciliano, "Autonomy in surgical robots and its meaningful human control," *Paladyn Journal of Behavioral Robotics*, vol. 10, no. 1, pp. 30–43, 2019.

[17] J. T. Bishoff and L. R. Kavoussi, *Atlas of Laparoscopic and Robotic Urologic Surgery E-Book*. Elsevier Health Sciences, 2016.

[18] A. Petit, F. Ficuciello, G. Fontanelli, L. Villani, and B. Siciliano, "Using physical modeling and rgb-d registration for contact force sensing on deformable objects," in *14th International Conference on Informatics in Control, Automation and Robotics*, vol. 2, 2017, pp. 24–33.

[19] C. P. Delaney, A. C. Lynch, A. J. Senagore, and V. W. Fazio, "Comparison of robotically performed and traditional laparoscopic colorectal surgery," *Diseases of the Colon & Rectum*, vol. 46, no. 12, pp. 1633–1639, 2003.

[20] J. W. Milsom, B. Böhm, and K. Nakajima, *Laparoscopic colorectal surgery*. Springer, 2006.

[21] T. Frank and A. Cuschieri, "Prehensile atraumatic grasper with intuitive ergonomics," *Surg Endosc*, vol. 11, no. 10, pp. 1036–1039, 1997.

[22] D. E. Litwin, A. Darzi, J. Jakimowicz, J. J. Kelly, D. Arvidsson, P. Hansen, M. P. Callery, R. Denis, D. L. Fowler *et al.*, "Hand-assisted laparoscopic surgery (HALS) with the handport system: initial experience with 68 patients," *Annals of surgery*, vol. 231, no. 5, 2000.

[23] D. Meijer, J. Bannenberg, and J. Jakimowicz, "Hand-assisted laparoscopic surgery," *Surgical Endoscopy*, vol. 14, no. 10, pp. 891–895, 2000.

[24] O. Ritsuya, T. Toshio, O. Toru, O. Toshiki, K. Kazuyuki, T. Kozo, and T. Naofumi, "Assemblable three fingered five-DoF hand for laparoscopic surgery," in *IEEE International Conference on Robotics and Automation*, 2008, pp. 3896–3901.

[25] T. Takayama, T. Omata, T. Futami, H. Akamatsu, T. Ohya, K. Kojima, K. Takase, and N. Tanaka, "Detachable-fingered hands for manipulation of large internal organs in laparoscopic surgery," in *IEEE International Conference on Robotics and Automation*, 2007, pp. 244–249.

[26] J. Gafford, Y. Ding, A. Harris, T. McKenna, P. Polygerinos, D. Holland, C. Walsh, and A. Moser, "Shape deposition manufacturing of a soft, atraumatic, and deployable surgical grasper," *Journal of Mechanisms and Robotics*, vol. 7, no. 2, pp. 021 006–021 006–11, 2015.

[27] A. Mirbagheri and F. Farahmand, "A triple-jaw actuated and sensorized instrument for grasping large organs during minimally invasive robotic surgery," *The International Journal of Medical Robotics and Computer Assisted Surgery*, vol. 9, no. 1, pp. 83–93, 2013.

[28] A. Tzemanaki, P. Walters, A. G. Pipe, C. Melhuish, and S. Dogramadzi, "An anthropomorphic design for a minimally invasive surgical system based on a survey of surgical technologies, techniques and training," *The International Journal of Medical Robotics and Computer Assisted Surgery*, vol. 10, no. 3, pp. 368–378, 2014.

[29] K. Yoshida, H. Yamada, R. Kato, T. Seki, H. Yokoi, and M. Mukai, "Development of five-finger robotic hand using master-slave control for hand-assisted laparoscopic surgery," in *IEEE Int. Conf. of the Engineering in Medicine and Biology Society*, 2016, pp. 5124–5127.

[30] M. Selvaggio, G. A. Fontanelli, V. R. Marrazzo, U. Bracale, A. Irace, G. Bregio, L. Villani, B. Siciliano, and F. Ficuciello, "The MUSHA underactuated hand for robot-aided minimally invasive surgery," *The International Journal of Medical Robotics and Computer Assisted Surgery*, p. e1981, 2018.

[31] T. Ortmaier, B. Deml, B. Kübler, G. Passig, D. Reintsema, and U. Seibold, *Robot Assisted Force Feedback Surgery*. Berlin, Heidelberg: Springer Berlin Heidelberg, 2007, pp. 361–379.

[32] S. McKinley, A. Garg, S. Sen, R. Kapadia, A. Murali, K. Nichols, S. Lim, S. Patil, P. Abbeel, A. M. Okamura, and K. Goldberg, "A single-use haptic palpation probe for locating subcutaneous blood vessels in robot-assisted minimally invasive surgery," in *IEEE International Conference on Automation Science and Engineering*, 2015, pp. 1151–1158.

[33] H. Liu, J. Li, X. Song, L. D. Seneviratne, and K. Althoefer, "Rolling indentation probe for tissue abnormality identification during minimally invasive surgery," *IEEE Transaction on Robotics*, vol. 27, no. 3, pp. 450–460, 2011.

[34] G. A. Fontanelli, L. R. Buonocore, F. Ficuciello, L. Villani, and B. Siciliano, "A novel force sensing integrated into the trocar for minimally invasive robotic surgery," in *IEEE/RSJ International Conference on Intelligent Robots and Systems*, 2017, pp. 131–136.

[35] P. Puangmali, H. Liu, L. D. Seneviratne, P. Dasgupta, and K. Althoefer, "Miniature 3-axis distal force sensor for minimally invasive surgical palpation," *IEEE/ASME Transactions on Mechatronics*, vol. 17, no. 4, pp. 646–656, 2012.

[36] R. Haslinger, P. Leyendecker, and U. Seibold, "A fiberoptic force-torque-sensor for minimally invasive robotic surgery," in *IEEE International Conference on Robotics and Automation*, 2013, pp. 4390–4395.

[37] U. Seibold, B. Kubler, and G. Hirzinger, "Prototype of instrument for minimally invasive surgery with 6-axis force sensing capability," in *IEEE International Conference on Robotics and Automation*, 2015.

[38] G. Tholey and J. P. Desai, "A modular, automated laparoscopic grasper with three-dimensional force measurement capability," in *IEEE International Conference on Robotics and Automation*, 2007, pp. 250–255.

[39] U. Kim, D.-H. Lee, W. J. Yoon, B. Hannaford, and H. R. Choi, "Force sensor integrated surgical forceps for minimally invasive robotic surgery," *IEEE Transactions on Robotics*, vol. 31, no. 5, pp. 1214–1224, 2015.

[40] U. Kim, Y. B. Kim, D.-Y. Seok, J. So, and H. R. Choi, "A surgical palpation probe with 6-axis force/torque sensing capability for minimally invasive surgery," *IEEE Transactions on Industrial Electronics*, vol. 65, no. 3, pp. 2755–2765, 2018.

[41] D.-H. Lee, U. Kim, T. Gulrez, W. J. Yoon, B. Hannaford, and H. R. Choi, "A laparoscopic grasping tool with force sensing capability," *IEEE/ASME Transactions on Mechatronics*, vol. 21, no. 1, pp. 130–141, 2016.

[42] U. Kim, Y. B. Kim, J. So, D.-Y. Seok, and H. R. Choi, "Sensorized surgical forceps for robotic-assisted minimally invasive surgery," *IEEE Transactions on Industrial Electronics*, vol. 65, no. 12, pp. 9604–9613, 2018.
[43] G. De Maria, C. Natale, and S. Pirozzi, "Force/tactile sensor for robotic applications," *Sensors and Actuators A: Physical*, vol. 175, pp. 60–72, 2012.
[44] P. Kazanzides, Z. Chen, A. Deguet, G. S. Fischer, R. H. Taylor, and S. P. DiMaio, "An open-source research kit for the da Vinci surgical system," *IEEE International Conference on Robotics and Automation*, pp. 6434–6439, 2014.
[45] Z. Chen, A. Deguet, R. H. Taylor, and P. Kazanzides, "Software architecture of the da Vinci research kit," in *IEEE International Conference on Robotic Computing*, 2017, pp. 180–187.
[46] G. A. Fontanelli, M. Selvaggio, M. Ferro, F. Ficuciello, M. Vendittelli, and B. Siciliano, "Portable dVRK: an augmented V-REP simulator of the da Vinci research kit," *Acta Polytechnica Hungarica*, vol. 16, no. 8, pp. 79–98, 2019.
[47] G. A. Fontanelli, F. Ficuciello, L. Villani, and B. Siciliano, "Modelling and identification of the da Vinci research kit robotic arms," in *IEEE/RSJ International Conference on Intelligent Robots and Systems*, 2017, pp. 1464–1469.
[48] G. A. Fontanelli, M. Selvaggio, M. Ferro, F. Ficuciello, M. Vendittelli, and B. Siciliano, "A V-REP simulator for the da vinci research kit robotic platform," in *IEEE International Conference on Biomedical Robotics and Biomechatronics*, 2018, pp. 1056–1061.
[49] Intuitive Surgical Inc., "Da vinci X/Xi instrument & accessory catalog," September 2019.

Huan Liu is currently a postdoctoral researcher with the ICAROS center (Interdepartmental Center for Advances in Robotic Surgery) of the University of Naples Federico II, Naples, Italy. He received the M.S. degree from the School of Power and Mechanical Engineering, Wuhan University, Wuhan, China, in 2010 and the doctoral degree from the School of Mechanical Engineering, Shanghai Jiao Tong University, Shanghai, China, in 2018. His research interests include prosthetic hands, surgical robotics and continuum mechanisms.

Mario Selvaggio is a Post Doc University of Naples Federico II, Naples, Italy. He received the Bachelor and the Master degrees (magna cum laude) in mechanical engineering from the same university in 2013 and 2015, respectively. In 2014, he was master student with the Fraunhofer IGD, Darmstadt, Germany. In 2016, he was intern with the Advanced Robotics department, Istituto Italiano di Technologia, Genova, Italy. He was visiting student with IRISA, INRIA Rennes in 2017 and 2018. In 2019, he was visiting student with the University of California Santa Barbara. His research activities focus on shared control, telerobotics, passivity-based control, grasping and manipulation.

Pasquale Ferrentino is currently a Ph.D. student at Vrije Universiteit Brussel, Brussels, Belgium. He received the Bachelor degree in biomedical engineering and the Master degree in Industrial Bioengineering from the University of Naples Federico II, Naples, Italy in 2016 and 2019, respectively. His research activities focus on modeling and control of soft robots.

Rocco Moccia is currently a Ph.D. candidate in Information Technology and Electrical Engineering at Università degli Studi di Napoli Federico II, Naples, Italy. He received the M.S. degree in mechanical engineering in 2017 from Sapienza, Università di Roma. In 2015, he was a master student with Human Neuromuscular Physiology Lab and Biorobotics and Human Modeling Lab at Georgia Institute of Technology. His research interests include surgical robotics, visual perception and shared control.

Salvatore Pirozzi is currently an Associate Professor with the University of Campania "Luigi Vanvitelli", Italy. He has authored or co-authored more than 70 international journal and conference papers. His research interests include modeling and control of smart actuators for active noise and vibration control, design and modelling of innovative sensors, in particular of tactile solutions, as well as interpretation and fusion of data acquired from the developed sensors. He is currently an Associate Editor for the IEEE Transactions on Control Systems Technology.

Umberto Bracale is an Associate Professor of general surgery at the University of Naples Federico II. His practical and research field of interest concerns laparoscopic and robotic treatment of benign and malignant gastrointestinal diseases. He did some stages and courses in important national and international institutions (University of Milano "San Raffaele", "San Camillo" Hospital of Trento, Maidstone Hospital in UK, University of Dundee and IRCAD of Strasbourg) to achieve competency in minimally invasive surgery. He is author of 60 scientific papers published in peer reviewed journals and he is editor of one Springer book. He is an Associate Editor of the Hernia Journal and the BMC Journal.

Fanny Ficuciello is an Assistant Professor with the University of Naples Federico II. She obtained the Laurea degree magna cum laude in Mechanical Engineering and the Ph.D. degree in Computer and Automation Engineering from the same university, in 2007 ans 2010 respectively. From 2009 to 2010, she was a Visiting Scholar with the Control Engineering Group, University of Twente, Enschede, The Netherlands. Her research interests include: design and control of anthropomorphic hands, grasping and manipulation, human-robot interaction, impedance-based control and redundancy resolution strategies, surgical robotics. She is the recipient of a National Grant within the "Programma STAR Linea 1" under which she is the PI of the MUSHA project. She is currently an Associate Editor for the IEEE Transactions on Robotics and the Journal of Intelligent Service Robotics.